Heterogeneous & Homogeneous & Bio- & Nano-

CHEMCATCHEM

CATALYSIS

Accepted Article

Title: Morphologically Cross-shaped Ru/HZSM-5 Catalyzed Tandem Hydrogenolysis of Guaiacol to Benzene in Water

Authors: Chen Zhao, Zhaoxia Zheng, and Zhicheng Luo

To be cited as: *ChemCatChem* 10.1002/cctc.201701398

Link to VoR: http://dx.doi.org/10.1002/cctc.201701398

A Journal of

ChemPubSoc Europe

WILEY-VCH

www.chemcatchem.org

Morphologically Cross-shaped Ru/HZSM-5 Catalyzed Tandem Hydrogenolysis of Guaiacol to Benzene in Water

Zhaoxia Zheng [a], Zhicheng Luo [a], Chen Zhao *[a]

Abstract: Hydrogenolysis of C-O bonds is an important tool for synthesis of valuable fuels and chemicals from biomass. In this contribution, we report that morphologically cross-shaped HZSM-5 loaded Ru nanoparticles have demonstrated a high activity in selective hydrogenolysis of guaiacol to benzene in water with a 97% yield and a rate of 7.8 $g \cdot g^{-1} \cdot h^{-1}$ accompanied with high durability. The N_2 sorption showed that Ru/HZSM-5 (cross-shaped) had the large mesoporous surface area and volume for loading small and uniform Ru nanoparticles, as confirmed by TEM images. The stronger interaction of Ru and cross-shaped HZSM-5 was simultaneously confirmed by a higher hydrogen-reduction temperature of RuO_2 on calcined Ru/HZSM-5, a blue shift of $Ru^{\delta+}$-$(CO)_n$, $Ru^{\delta+}$-(CO), and Ru^0-(CO) species in IR spectra of adsorbed CO, and a higher Ru $3d_{5/2}$ binding energy in X-ray photoelectron spectroscopy measurements. The reaction constant in guaiacol hydrogenolysis to phenol over cross-shaped Ru/HZSM-5 (0.051 min^{-1}) was 3-4 times higher than that on spherical and cuboid Ru/HZSM-5 (0.012-0.029 min^{-1}) at identical conditions, attributed to the remarkable hydrogenolysis catalytic capability of Ru nanoparticles on cross-shaped HZSM-5. In addition, adsorption of guaiacol and hydrogen was more substantial on cross-shaped Ru/HZSM-5, as evidenced by respective detectors of Infrared and mass spectroscopy. The higher adsorption of guaiacol is attributed to the abundant Lewis acid sites (LAS) on cross-shaped Ru/HZSM-5, as the Al-OH enriched LAS favor for the adsorption of oxygen-containing guaiacol. The higher rate-constant in the primary step, together with the adsorbed high concentrated reactant and hydrogen (with nearly first reaction orders) on cross-shaped Ru/HZSM-5 facilitates the tandem rates in such reaction to some extent, leading to an excellent hydrogenolysis catalyst working at hydrothermal conditions for biomass conversion.

Introduction

Guaiacol is a representative phenolic compound derived from lignin depolymerization,[1] anchoring about two oxygen-containing functional groups: phenolic hydroxyl and phenolic methoxy groups. Catalytic hydrodeoxygenation (HDO) is a useful upgrading approach to convert phenolic mixture to fuels or chemicals.[2] Compared to the fully hydrodeoxygenated products of alkanes, aromatic hydrocarbons are shown to be more attractive with higher energy density as important chemical intermediate. Selective HDO of guaiacol to benzene is quite challenging,[3] as the reactant as well as intermediates and products tends to be hydrogenated to saturated compounds in the hydrogen atmosphere.

In the gas phase, sulfide and non-sulfide catalysts were used for guaiacol HDO to aromatic hydrocarbons. Sulfide catalysts such as NiMoS[4] and CoMoS[5] can catalyze aromatic hydrocarbons production with high selectivity, but they are susceptible to deactivate in presence of water. In addition, non-sulfide catalysts including metal catalysts such as Pt,[6] Ni, [7] Fe, [8] Mo, [9] can be used to catalyze the selective HDO route in the gas phase. Especially with Mo/C[9] or PdFe/C, [10] the selectivity of aromatic hydrocarbon can be up to 80%. In addition, MoN_2, [11] MoO_3-NiO[12] and NiP/SiO_2[13] can also catalyze arenes from guaiacol.

Water is wildly present in the biomass and in the HDO product, and thus, the role of water as a suitable solvent should be addressed for guaiacol HDO. In aqueous hydrothermal conditions, our group have developed Ru/sulfate zirconia[14] and Ru/HZSM-5 catalysts[15] for selectively HDO of phenolic monomers and phenolic dimers to arenes. We also found that in the presence of hydrogen, highly selective hydrogenolysis without hydrogenation depends on the concentration and intensity of H· adsorption during the reaction. Thus, the high temperature and low hydrogen pressure environment is beneficial to remove substantial H· species on the surface. In that case, it not only reduces the surface H· concentration, but also changes the spatial H· distribution on the surface. In addition, Fu et al[16] also reported a similar Ru-WO_x/SiAl catalyst system to convert of phenols and phenyl ethers to arenes in high-temperature water.

It is well recognized that hydrogenolysis is catalyzed by the metal site, but the capability of metal would be dramatically influenced by the support. Herein, we reported that morphologically cross-shaped HZSM-5 loaded Ru nanoparticles showed a high activity as well as high stability in selective hydrogenolysis of guaiacol to benzene in a tandem step via phenol intermediate in presence of high temperature (240 °C) and a low hydrogen pressure (2 bar) in the water phase. Extensive ex situ characterization and adsorption measurements were performed in order to explain the best hydrogenolysis performance on cross-shaped Ru/HZSM-5.

Results and Discussion

Comparison of three Ru/HZSM-5 samples with different morphologies

The Ru based catalysts have demonstrated relatively high selectivity in hydrogenolysis of C-O bonds of bio-molecules such as phenols, glycerol, cellulose, and lignin. Here in the present

[a] *Zhaoxia Zheng, Zhicheng Luo, Prof. Dr. Chen Zhao*
Shanghai Key Laboratory of Green Chemistry and Chemical Processes, Department of Chemistry, East China Normal University, Shanghai 200062, China
E-mail: czhao@chem.ecnu.edu.cn

Supporting information for this article is given via a link at the end of the document.

work, three HZSM-5 samples with different morphologies (cross-shaped, spherical, and cuboid) with comparable Si/Al_2 ratios of 80 to 120 were synthesized for loading Ru nanoparticles in the investigation of guaiacol hydrogenolysis to benzene at the hydrothermal conditions. Three catalysts are annotated as Ru/HZSM-5(100)-1 (cross-shaped), Ru/HZSM-5(80)-2 (spherical), and Ru/HZSM-5(120)-3 (cuboid), respectively. The Ru nanoparticles are incorporated by the incipient wetness impregnation method, with comparable loadings of ca. 5 wt% as detected by inductively coupled plasma (ICP) analysis. The morphologies of three samples were measured by scanning electron microscope (SEM), as shown in Figure 1. HZSM-5(100)-1 comprised of numerous cross-shaped crystals with uniform size of ca. 1-2 μm, while HZSM-5(80)-2 was consisted by 3-4 nm spherical small particles to construct into separate large crystals (7-8 μm). In comparison, HZSM-5(120)-3 was made up by regular cuboid-shaped particles with average sizes of 1-2 μm. The morphological disparity may dramatically influence the properties of supports such as surfaces, pore structures, acidity, and in addition to the properties of metals.

The summarized data for physicochemical and acid properties of three HZSM-5 and Ru/HZSM-5 catalysts are compiled in Table S1 and Table 1. The N_2 adsorption/desorption data demonstrated that the micropore structures of three Ru/HZSM-5 samples were quite similar, with S_{micro} of 254-283 $m^2 \cdot g^{-1}$ and V_{micro} of 0.13-0.14 $cm^3 \cdot g^{-1}$. However, it was noted that their mesopores structures were different. The S_{meso} surface areas were 132, 61, and 29 $m^2 \cdot g^{-1}$ for Ru/HZSM-5(100)-1, Ru/HZSM-5(80)-2, Ru/HZSM-5(120)-3, respectively. In an accordance, the S_{meso} volumes were respectively decreased from 0.49, 0.16, to 0.07 $cm^3 \cdot g^{-1}$.

The acidic sites of three Ru/HZSM-5 samples were detected by IR spectra of adsorbed pyridine. Shown from the IR results, the Brönsted acid sites of three samples were very close at the range of 0.213-0.268 $mmol \cdot g^{-1}$. Whereas Lewis acid site of cross-shaped Ru/HZSM-5(100)-1 (0.030 $mmol \cdot g^{-1}$) was two or three times higher than that on Ru/HZSM-5(80)-2 and Ru/HZSM-5(120)-3 (0.010-0.014 $mmol \cdot g^{-1}$). The abundant Lewis acid sites on HZSM-5(100)-1 may greatly influence the adsorption of guaiacol reactant, and then dramatically affect the corresponding hydrogenolysis rate on the assumption of first-order reaction towards guaiacol concentration.

Subsequently, the particle information of Ru on three samples was analyzed by XRD patterns and TEM images. The diffraction peaks of 38.4°, 42.2° and 44.0° in XRD patterns were assigned to hexagonal close-packed (hcp)-structured Ru (100), Ru (002) and Ru (101) facets, respectively (Figure 2). It was obviously observed that Ru/HZSM-5(120)-3 had a mixture of hexagonal close-packed Ru (100), Ru (002) and Ru (101) facets, while Ru/HZSM-5(80)-2 contained a Ru (101) phase, and no Ru diffraction peaks was shown for Ru/HZSM-5(100)-1. Based on the Scherrer equation for XRD patterns, this indicates that the Ru nanoparticle sizes on three samples would follow the increasing order, Ru/HZSM-5(100)-1 < Ru/HZSM-5(80)-2 < Ru/HZSM-5(120)-3. In line with this result, TEM images showed the average Ru particles on Ru/HZSM-5(100)-1, Ru/HZSM-5(80)-2, and Ru/HZSM-5(120)-3 were 4.0±0.9, 4.5±0.8, 5.0±0.7 nm (Figure S1, Table 1). It can be also inferred that the small and uniform Ru nanoparticles on the cross-shaped HZSM-5 maybe resulted from the high mesoporous surface area and pore volume of the support.

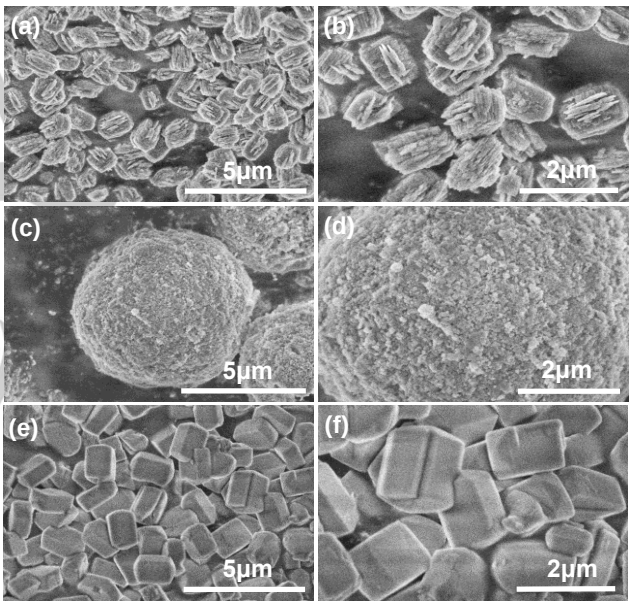

Figure 1. SEM images of (a-b) HZSM-5(100)-1, (c-d) HZSM-5(80)-2, and (e-f) HZSM-5(120)-3.

Table 1. The characterized physicochemical and acidic properties of three Ru/HZSM-5 samples.

Ru/HZSM-5	Si/Al_2[a] ($mol \cdot mol^{-1}$)	S_{meso}[b] ($m^2 \cdot g^{-1}$)	S_{micro}[b] ($m^2 \cdot g^{-1}$)	V_{meso}[b] ($cm^3 \cdot g^{-1}$)	V_{micro}[b] ($cm^3 \cdot g^{-1}$)	D_{Ru}[c] (nm)	Acid conc. (Py-IR) ($mmol \cdot g^{-1}$)	
							BAS	LAS
1	100	132	256	0.49	0.13	4.0±0.9	0.251	0.030
2	80	61	254	0.16	0.13	4.5±0.8	0.213	0.010
3	120	29	283	0.07	0.14	5.0±0.7	0.268	0.014

[a] Detected by ICP.
[b] Determined by N_2 sorption.
[c] Calculated by TEM images.

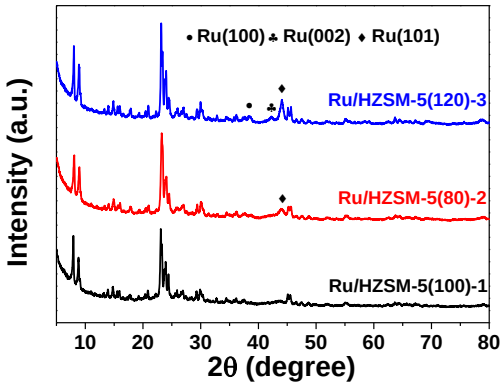

Figure 2. XRD patterns of Ru/HZSM-5(100)-1, Ru/HZSM-5(80)-2, and Ru/HZSM-5(120)-3.

In a next step, the interaction of Ru and HZSM-5 support was investigated by temperature programmed reduction of hydrogen (TPR-H_2), IR spectra of adsorbed CO (IR-CO), and X-ray photoelectron spectroscopy (XPS) measurements. As shown from the TPR-H_2 profile in Figure 3a, the strong reduction peaks at 120-190 °C were assigned to reduction of the RuO_2 species on the surface. The maximum peaks in reduction temperatures of RuO_2 in Ru/HZSM-5(100)-1, Ru/HZSM-5(80)-2 and Ru/HZSM-5(120)-3 were located at 156, 140, and 128 °C, respectively. The highest reduction temperature for RuO_2 (156°C) on cross-shaped HZSM-5-1 support implies the strongest interaction of metal and support.

The IR spectra of adsorbed CO (Figure 3b) showed three groups of adsorbed CO bands on Ru nanoparticles: HF_1 (high-frequency 1) at 2156-2133 cm^{-1}, HF_2 (high-frequency 2) at 2100-2060 cm^{-1}, and LF (low-frequency) bands at about 2040 ± 40 cm^{-1}, which were attributed to $Ru^{\delta+}$-$(CO)_n$, $Ru^{\delta+}$-(CO), and Ru^0-(CO) species, respectively. [17] The main bands of $Ru^{\delta+}$-$(CO)_n$ of Ru/HZSM-5(100)-1, Ru/HZSM-5(80)-2, and Ru/HZSM-5(120)-3 were located at 2135, 2130 and 2128 cm^{-1}, respectively. Obviously, there showed a blue shift from Ru/HZSM-5(120)-3 to Ru/HZSM-5(100)-1 for $Ru^{\delta+}$-$(CO)_n$ species. In a same trend, the bands assigned to $Ru^{\delta+}$-(CO) and Ru^0-(CO) also showed the similar shift. In general, a blue shift in IR spectra indicates relatively high transition energy of adsorbed CO species on Ru surface. The relatively high transition energy of $Ru^{\delta+}$-$(CO)_n$, $Ru^{\delta+}$-(CO), and Ru^0-(CO) species can be resulted from the strong interaction of Ru and HZSM-5 support, as confirmed by the results from TPR-H_2 profile. The strong interaction may be due to the electron transfer from Ru to HZSM-5(100)-1 support, and consequently, an electron-deficient Ru metal center is formed.

XPS was used to illuminate the structural and chemical state of Ru on the HZSM-5 surface. As shown in Figure 3c, the main peak at 284.8 eV was assigned to the strong signal from carbon. The binding energy (BE) for Ru $3d_{5/2}$ on Ru/HZSM-5(100)-1, Ru/HZSM-5(80)-2, and Ru/HZSM-5(120)-3 was 280.8, 280.5, and 280.2 eV, respectively. It is demonstrated that the shift of three samples to higher binding energy of Ru^0 is due to different metallic Ru(0) states. The highest binding energy of Ru $3d_{5/2}$ demonstrates a highest electronegativity on Ru resulted from the strongest Ru and HZSM-5 interaction. This is in an agreement with the results from IR spectra of adsorbed CO and TPR profile of adsorbed H_2.

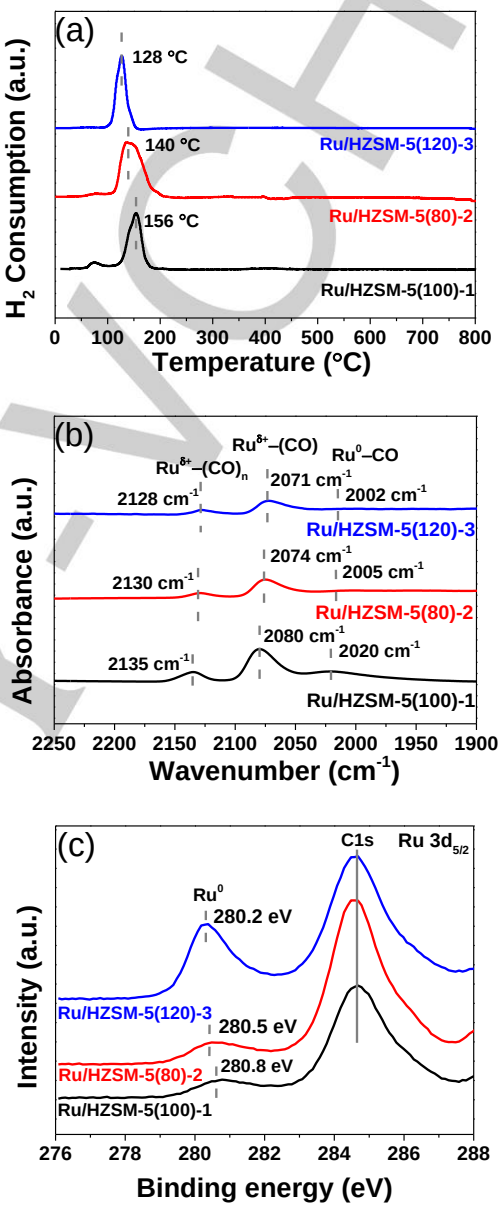

Figure 3. (a) TPR-H_2 profile, (b) IR spectra of adsorbed CO, and (c) Ru $3d_{5/2}$ XPS spectra of three Ru/HZSM-5 samples.

Evaluation of the catalytic performances for tandem hydrogenolysis of guaiacol to benzene over three Ru/HZSM-5 samples

The hydrogenolysis of guaiacol was evaluated on three Ru/HZSM-5 catalysts in water with a fixed guaiacol and catalyst ratio of 20 $g \cdot g^{-1}$. The conditions with a high temperature and a low pressure (240 °C and 2 bar H_2) was adopted, since the adsorbed few H· species nearby the oxygen atom of guaiacol is more strongly adsorbed under such conditions and thus

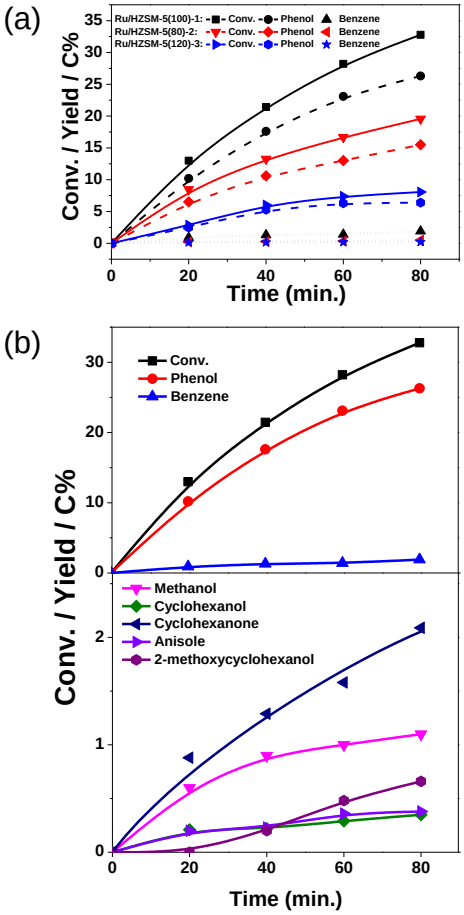

Figure 4. (a) Kinetics of hydrogenolysis of guaiacol over three Ru/HZSM-5 catalysts. (b) The product distributions on guaiacol hydrogenolysis over Ru/HZSM-5(100)-1 as a function of time. General conditions: guaiacol (1.0 g), Ru/HZSM-5 catalyst (0.05 g), H_2O (100 mL), 240 °C, 2 bar H_2 and 6 bar N_2, stirring at 600 rpm.

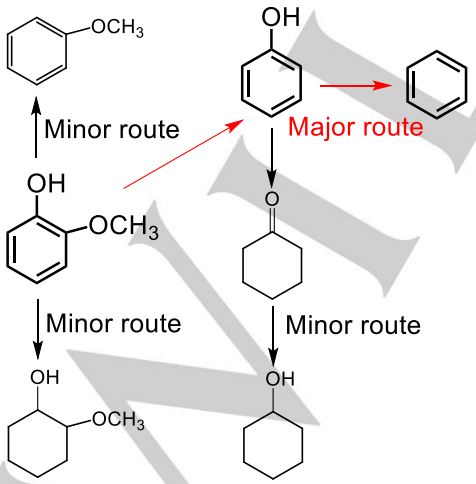

Scheme 1. The proposed plausible routes on guaiacol hydrogenolysis over Ru/HZSM-5 in presence of hydrogen.

preferred to be retained on the Ru surface.[18] Therefore, selective hydrogenolysis of the CH_3O-Ar bond is successfully conducted at such conditions.

The plotted kinetics curves for guaiacol hydrogenolysis over three Ru/HZSM-5 samples were displayed were in Figure 4a and Table S2. After a reaction time of 80 min., the conversion values attained 33%, 20% and 8%, respectively, on Ru/HZSM-5(100)-1, Ru/HZSM-5(80)-2 and Ru/HZSM-5(120)-3. The gained initial rates were 63, 41, 14 $mmol \cdot g^{-1} \cdot h^{-1}$, correspondingly. The carbon balance in the liquid phase exceeded 93% in the liquid phase. In addition, it was noted that primary product was phenol with the high selectivity of guaiacol to phenol over three Ru/HZSM-5 samples, which was originated from Ar-OCH_3 bond (bond dissociation energy: 409-421 kJ/mol) cleavage of guaiacol. The yields of benzene were then attained at 8%, 6%, and 0.2% at 80 min..

Apart from the primary phenol and its hydrogenated products cyclohexanone and cyclohexanol from guaiacol conversion, other products including benzene, anisole, 2-methoxycyclohexanol, and methanol were also detected with Ru/HZSM-5(100)-1 (Figure 4b). Based on this information, it can be concluded that the main pathway for guaiacol conversion proceeds with in tandem hydrogenolysis to phenol and methanol, and subsequently phenol is cleaved into benzene and water. The phenol intermediate can be also hydrogenated to cyclohexanone and cyclohexanol in a minor part (Scheme 1). In addition, Guaiacol can be also hydrogenolyzed to anisole or hydrogenated to 2-methoxycyclohexanol as by-products. Thus, the crucial factor in achieving the high selectivity of benzene is to enhance the tandem hydrogenolysis capability on Ru center.

It has been demonstrated that the reaction orders for hydrogen and guaiacol concentrations were 0.74 and 0.97, respectively.[15] Since the hydrogen pressure before and after the reaction was almost unchanged, the parameter for the hydrogen pressure can be considered to be a constant. The reaction order for the guaiacol concentration (0.97) approached 1, and therefore, the reaction steps and individual reaction equation from guaiacol hydrogenolysis to phenol, and then hydrogenolysis to benzene can be drawn in Figure 5a and Figure 5b.

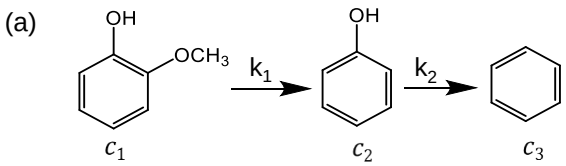

(b)

$$\frac{dc_1}{dt} = -k_1 \times c_1$$

$$\frac{dc_2}{dt} = k_1 \times c_1 - k_2 \times c_2$$

$$\frac{dc_3}{dt} = k_2 \times c_2$$

Figure 5. (a) A first-order reaction on tandem hydrogenolysis of guaiacol to benzene. (b) Individual reaction equations for the hydrogenolysis of guaiacol to benzene. General conditions: guaiacol (1.0 g), Ru/HZSM-5 (0.05 g), H_2O (100 mL), 240 °C, 2 bar H_2 and 6 bar N_2, stirring at 600 rpm.

The Matlab software is used to simulate the kinetics curve for the tandem hydrogenolysis of guaiacol to benzene via phenol intermediate. As shown in Table 2, the curves simulated by Matlab software are fitted well with the kinetics curves over three Ru/HZSM-5 catalysts. The fitted reaction constants for the individual steps are listed in Table 2.

With the Ru/HZSM-5-1 sample, the initial rate constant for hydrogenolysis of guaiacol to phenol (k_1 = 0.0051 min^{-1}) was much higher than the second step for hydrogenolysis of phenol to benzene (k_2 = 0.0034 min^{-1}). In comparison to other two Ru/HZSM-5 catalysts, the gained rates for the first step for converting of guaiacol to phenol were 0.0051, 0.0029, and 0.0012 min^{-1}, respectively. This implies the first hydrogenolysis step rate on Ru/HZSM-5(100)-1 was two or three times higher than that on other two Ru samples. The rate constants for the second step of forming benzene from phenol were quite similar at 0.0034, 0.0033, and 0.0030 min^{-1}. In general, the higher rate constant of k_2 than k_1 indicates that the initial step for hydrogenolysis of guaiacol is the rate-limiting step on Ru/HZSM-5 catalysts. The higher rate-constant in the two steps of guaiacol hydrogenolysis on cross-shaped Ru/HZSM-5(100)-1 may be attributed to the remarkable capability of supported Ru nanoparticles.

Table 2. Fitted curves and rate constants (*k*) for hydrogenolysis of guaiacol to benzene over three Ru/HZSM-5 simulated by Matlab software.

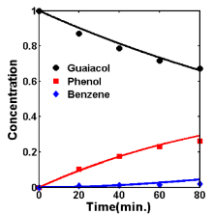

Ru/HZSM-5(100)-1

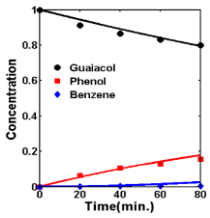

Ru/HZSM-5(80)-2

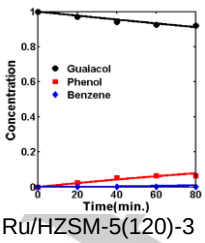

Ru/HZSM-5(120)-3

Catalyst	k_1 (min^{-1}) guaiacol to phenol	k_2 (min^{-1}) phenol to benzene
Ru/HZSM-5(100)-1	0.0051	0.0034
Ru/HZSM-5(80)-2	0.0029	0.0033
Ru/HZSM-5(120)-3	0.0012	0.0030

Later, the temperature dependence at the range from 180 to 220 °C towards the tandem hydrogenolysis of guaiacol was explored over Ru/HZSM-5(100)-1 in presence of 2 bar H_2 (Figure S3). With a temperature increase from 180 to 240 °C, the conversion of guaiacol gradually increased from 21%, to 28%, 30%, and 33% at 80 min., suggesting low temperature dependence towards the rate increase.

The Arrhenius plot is thus acquired based the hydrogenolysis rate of the reaction at different temperatures (Figure S4). On the basis of Arrhenius's law ($lnk = lnA - E_a/RT$), we calculated the apparent activation energy (E_a) of this reaction to be 16.6 kJ·mol^{-1}. The small value of E_a indicates the hydrogenolysis rates with a low hydrogen pressure (2 bar) show a low temperature dependence at the selected temperature range. In addition, the apparent activation energy and the true activation energy shows the following relationship: $E_a^{obs} = E_a^{true} + (1-\theta_A)\cdot\Delta H_A$. Since the reaction pressure is low (2 bar) under the current catalytic system, the value of θ_A is approximately 0. The formula can be simplified as $E_a^{obs} = E_a^{true} + \Delta H_A$. When guaiacol is preferentially adsorbed on Ru, the adsorption energy (ΔH_A) is -237 kJ·mol^{-1} at the corrected zero-point energy.[19] Therefore, the true activation energy of hydrogenolysis of guaiacol at selected conditions is calculated to be close to 253.6 kJ·mol^{-1}.

Understanding the high activity of cross-shaped Ru/HZSM-5(100)-1 for tandem hydrogenolysis of guaiacol to benzene

Afterwards, we try to explore the reason for the high activity of cross-shaped Ru/HZSM-5(100)-1 for hydrogenolysis of Ar-OCH_3 bonds of guaiacol. The rate for guaiacol hydrogenolysis follows the equation I:

$$v = k[Guaiacol]^a[H_2]^b \ (a, b > 0)$$

(Equation I)

The rate constant *k* stands for the hydrogenolysis capability on the active site of Ru center. In the part of understanding the individual steps in guaiacol to benzene, it has been demonstrated that the calculated rate constant (0.0051 min^{-1}) on cross-shaped Ru/HZSM-5(100)-1 for the primary step was two or three times higher than that on other two catalysts (0.0029 and 0.0012 min^{-1}). The higher capability for C-O bond cleavage on supported Ru nanoparticles of cross-shaped HZSM-5(100)-1 maybe resulted from the smaller and more uniform particles on the high mesoporous surface areas of HZSM-5(100)-1, as well as strong Ru and HZSM-5 interaction. The smaller size of Ru nanoparticles is verified by TEM images and XRD patterns, and the stronger interaction of Ru and the cross-shaped HZSM-5 support is confirmed by a higher reduction temperature in TPR-H_2 profile, a blue shift in IR spectra of absorbed CO, a stronger electronegativity of Ru.

We used the method of IR spectra of absorbed guaiacol in the gas phase in vacuum to reflect the adsorption of guaiacol over three Ru/HZSM-5 samples in the aqueous phase at Figure 6a. Three main bands at 1500-1620 cm^{-1} were assigned to ν(C-C_{ring}) vibrations.[20] The ratios of integrated areas of guaiacol adsorption intensities at 1508, 1597 and 1619 cm^{-1} were 2.02:1.56:1 for three Ru/HZSM-5 samples sequentially, showing that the guaiacol adsorption capacity is substantially abundant on Ru/HZSM-5(100)-1. The much higher guaiacol adsorption is attributed to the Al-OH enriched Lewis acid sites on the support, as this electron-positive Al center can favorably adsorb the electron-negative Ar-OCH_3 and Ph-OH groups. [21] The higher Lewis acids on cross-shaped HZSM-5(100)-1 are also demonstrated by the IR spectra of absorbed pyridine as shown in Figure S2. To prove this point, we also tested the adsorption of guaiacol in the gas phase (Figure 6a) on the pure γ-Al_2O_3, and the result revealed that the adsorption intensity of guaiacol in IR spectrum was highly strong at 1508, 1597 and 1619 cm^{-1} with the Lewis Al center. This again demonstrates the higher guaiacol on cross-shaped HZSM-5(100)-1 is due to its abundant Lewis acid sites.

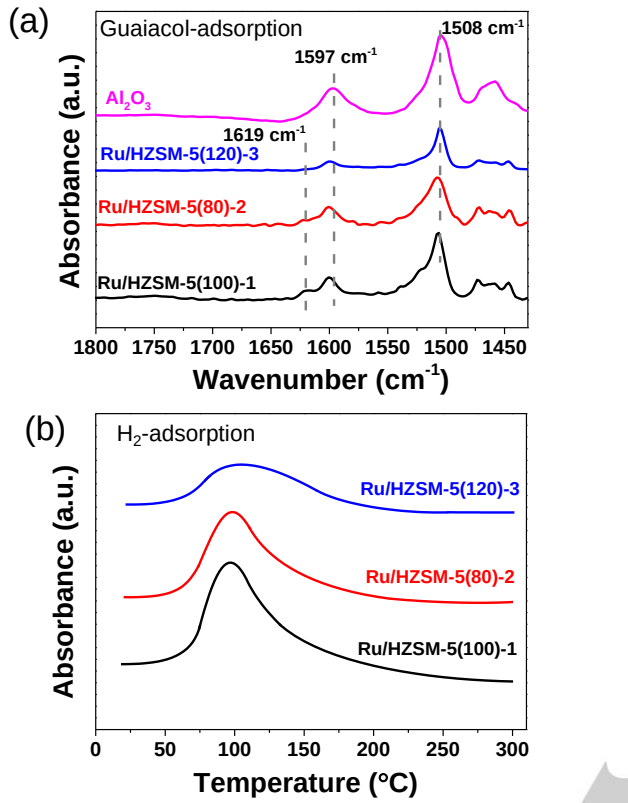

Figure 6. (a) The IR spectra of absorbed guaiacol, and (b) TPD/H_2-MS profiles of three Ru/HZSM-5 samples.

In addition, the adsorption of another reactant (hydrogen) is monitored by TPD/H_2-MS technique on three Ru/HZSM-5 samples (Figure 6b). The maximum desorption temperatures for adsorbed hydrogen located at around 100-110 °C. The ratios of adsorbed H_2 capacity of were 1.29:1.12:1 for three Ru/HZSM-5 samples. Basically, it is recognized that H_2 is adsorbed on the Ru nanoparticles, suggesting more accessible Ru nanoparticles on cross-shaped HZSM-5(100)-1. Therefore, based on the equation of $r = k\,[\text{guaiacol}]_{ads}^{a}[H_2]_{ads}^{b}$, the higher adsorbed reactants of guaiacol and hydrogen on the surface together with the high hydrogenolysis capability on cross-shaped Ru/HZSM-5(100)-1 (with *a* was 0.97 and *b* was 0.74) construct a promising hydrogenolysis catalyst.

Catalytic and recycling tests

To test the maximum benzene production capability from guaiacol, three Ru/HZSM-5 catalysts were compared at the identical conditions (240 °C, 2 bar H_2) for 1 h. The cross-shaped Ru/HZSM-5(100)-1 attained nearly quantitative benzene formation from guaiacol with a 97% yield of benzene and a 3% yield of methanol (Figure 7a and Table S3), while the yields of benzene only attained around 20% for Ru/HZSM-5(80)-2 and Ru/HZSM-5(120)-3 sample. These data again demonstrate the super high hydrogenolysis activity of Ru nanoparticles on cross-shaped HZSM-5.

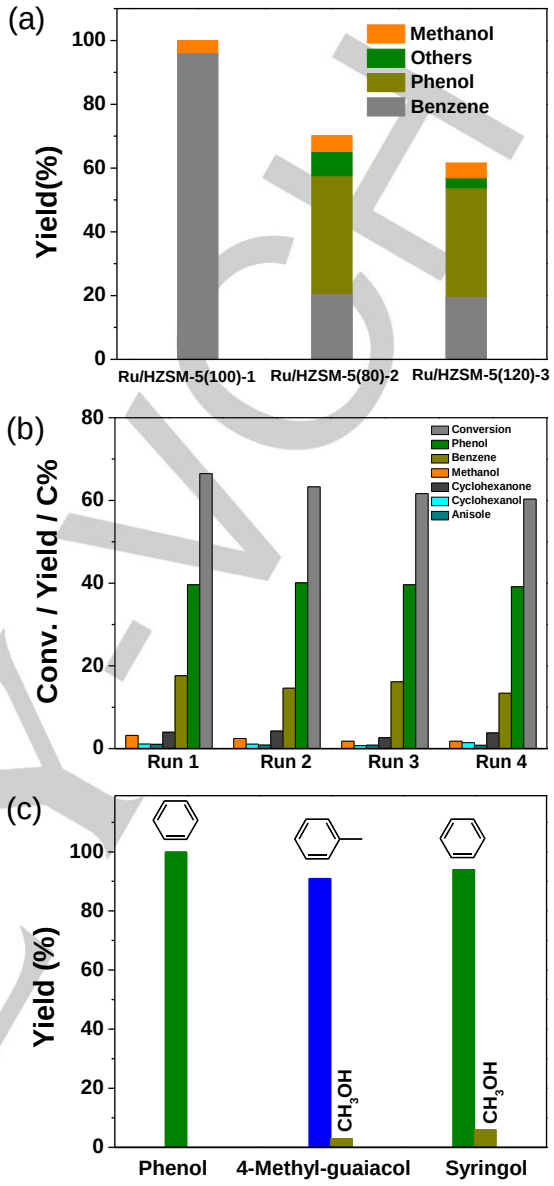

Figure 7. (a) The product distributions on conversion of guaiacol to benzene on three Ru/HZSM-5 samples, others refer to the products of cyclohexanone and cyclohexanol. Reaction conditions: guaiacol (0.2 g), Ru/HZSM-5 (0.2 g), H_2O (100 mL), 240 °C, 2 bar H_2 and 6 bar N_2, 1 h, stirring at 600 rpm. (b) Recycling test of the hydrodeoxygenation of guaiacol over Ru/HZSM-5(100)-1. Reaction conditions: guaiacol (1.0 g), Ru/HZSM-5(100)-1 (0.2 g), H_2O (100 mL), 240 °C, 2 bar H_2 and 6 bar N_2, 1 h, stirring at 600 rpm. (c) Selective hydrodeoxygenation of lignin-derived phenolic monomers (phenol, 4-methylguaiacol, and syringol) to aromatic hydrocarbons over Ru/HZSM-5(100)-1. Reaction conditions: reactant (0.2 g), Ru/HZSM-5(100)-1 (0.2 g), H_2O (100 mL), 240 °C, 2 bar H_2 and 6 bar N_2, stirring at 600 rpm, reaction time: 1 h for phenol, 4 h for 4-methyl-guaiacol and syringol.

The durability of the best Ru/HZSM-5(100)-1 catalyst was tested with four reaction cycles under this selected reaction condition. After each reaction, the catalyst was filtered and then dried in vacuum for the next use. As shown in Figure 7b and

Table S4, the conversion of guaiacol within 1 h was from 66% (fresh catalyst) to 63% (second cycle) and then to 62% (in the third cycle) and 60% (in the fourth cycle), whereas the conversion of the main products of phenol and benzene was essentially maintained at a level of 40% and 20% in each cycle. These results indicate that the catalyst is relatively stable under this harsh hydrothermal condition. In addition, the reactant was extended to diverse lignin derived monomers (phenol, 4-methylguaiacol, and syringol), and they were quantitatively converted to arenes at similar conditions (Fig. 7c). This suggests that the developed catalytic system is versatile for arenes production from hydrodeoxygenation of lignin pyrolysis oil.

Conclusions

The hydrogenolysis of cellulose, lignin, and lipids is wildly used in biomass conversion to produce fuels and chemicals. Here, we reported that Ru nanoparticles supported on cross-shaped HZSM-5 catalyzed a selective benzene production with a 97% yield from the hydrogenolysis of guaiacol at hydrothermal conditions in presence of a high temperature and a low hydrogen pressure (240 ºC, 2 bar H_2), with sequential rate constants of 0.0051 and 0.0034 min^{-1} for steps of guaiacol to phenol and phenol to benzene in a tandem reaction.

The characterization results show that the large mesoporous surface area and the mesopore pore volume of the cross-shaped HZSM-5 support was loaded with small and uniform Ru nanoparticles. The strong interaction between Ru and cross-shaped HZSM-5 support (as confirmed by TPR-H_2) leads to an electron-deficient Ru (as shown in IR spectra of adsorbed CO) and a strong electronegative Ru (as measured by XPS). Resultantly, cross-shaped Ru/HZSM-5 led to the overall highest rate constant in hydrogenolysis of guaiacol to phenol. In addition, the higher adsorbed reactants of guaiacol and hydrogen on the surface of cross-shape HZSM-5 together with the high hydrogenolysis capability on cross-shaped Ru/HZSM-5 construct a promising hydrogenolysis catalyst, offering high potentials for used in selective hydrogenolysis of diverse $C_{aliphatic}$-O and $C_{aromatic}$-O bonds in biomass at hydrothermal conditions.

Experimental Section

Materials

All chemicals were used without further purification: $RuCl_3 \cdot 3H_2O$ (J&K, ≥ 59.5 wt%), tetra-propylammonium hydroxide (TPAOH, Sinopec Co., Ltd., 25 wt%), tetra-ethylorthosilicate (TEOS, Sinopec Co., Ltd., containing 28.4 wt% SiO_2), tetraethylammonium bromide (TEABr, Alfa, 98 wt%), colloidal silica (Sigma-Aldrich, 30 wt%), piperidine (Aladdin, ≥99.5% analytical standard), aluminum sulfate octadecahydrate (Aladdin, 98.0%–102.0% ACS reagent), sodium hydroxide (Alfa Aesar, 98.0% flake). Guaiacol (Sinopharm, > 98% GC assay), ethyl acetate (Sinopharm, AR), phenol (Sinopharm, AR), 4-methylguaiacol (J&K, > 99% GC assay), 2,6-dimethoxy-4-methyl-phenol (Alfa Aesar, > 97% GC assay). Air, H_2, and N_2 gases (99.999 vol.%) were supplied by Shanghai Pujiang Specialty Gases Co., Ltd.

Synthesis of Cross-shaped HZSM-5

Cross-shaped HZSM-5 zeolites were synthesized with the assistant of active seeds[22]. Firstly, tetra-ethyl orthosilicate (TEOS) was dropped into the solution including water and tetrapropylammonium hydroxide (TPAOH, 25 wt%). After mixing at 353 K for 2 h, the gel (1.0 TEOS : 0.15 TPAOH : 14 H_2O) was introduced into a Teflon-lined steel autoclave, aging at 393 K for 3 h.

Piperidine (PI) was used as structure directing agent to synthesize HZSM-5 zeolite Sodium hydroxide and aluminum sulfate were first dissolved in the water. Then piperidine was added in the above solution. Next, silica sol and active seeding gel were dropped into the mixed solution and further stirred for 30 minutes, forming a gel composition of 1.0 SiO_2 : 0.01 Al_2O_3 : 0.2 PI : 0.05 Na_2O : 25 H_2O. SiO_2 in the active seeding gel accounted for 1 % of the whole SiO_2 in gel. The gel was crystallized in a Teflonlined steel autoclave at 443 K for 72 h. The ZSM-5 product was collected by filtration followed by washing with distilled water several times, dried at 373 K, and then calcined in air at 823 K for 6 h. The ZSM-5 was brought into ammonium form. After filtration, washing and drying at 373 K, the ammonium ion-exchanged zeolite was subsequently calcined at 823 K for 6 h to give HZSM-5.

Synthesis of Spherical HZSM-5

For spherical HZSM-5 synthesis, AIP was dissolved in a mixture of TPAOH and distilled water with stirring at ambient temperature for 2 h. Then TEOS was added drop-wise into the above solution, with a molar composition of 1 SiO_2 : 80 Al_2O_3 : 15 H_2O : 0.25 TPAOH, stirring for 4 h. The solution was transferred into a Teflon-lined stainless steel autoclave and crystallization in an oven lasted for 72 h at 170 ^oC. After cooling, the solid product was washed to neutrality, and sequentially centrifugated to remove supernatant liquid, and finally collected after drying at 110 ^oC overnight. Prior to use, it was calcined in flowing air (flowing rate: 100 $mL \cdot min^{-1}$) at 550 ^oC for 6 h.

Synthesis of Cuboid HZSM-5

Cuboid HZSM-5 zeolites were also synthesized with the assistant of active seeds[23]. The colloidal silica was added into the tetrapropylammonium hydroxide solution at room temperature, stirring for 4 h. Then the mixture (SiO_2 : 0.35 TPAOH : 19.6 H_2O) was transferred into the Teflon-lined stainlesssteel autoclave and hydrothermally treated at 353 K for 72 h. The obtained seeding gel was directly used for the synthesis of parent HZSM-5.

The $Al_2(SO_4)_3$ was dissolved in the sulfuric acid solution as the aluminum source. Then the solution was added into the water glass (SiO_2, 27.10 wt%; Na_2O, 8.39 wt%), after that the template tetraethylammonium bromide and seeding gel (the active seeding gel accounted for 0.5 % of the whole SiO_2 in gel)was added to obtain amixture with amolar composition of SiO_2 : 1/120 Al_2O_3 : 0.05 Na_2O : 0.05 TEABr : 30 H_2O. After hydrothermal synthesis at 458 K for 24 h, the resultant solid product was recovered by filtration, being washed with deionized water for several times and dried at 373 K overnight. The template was removed by the calcination at a ramp of 2 K min^{-1} to 823 K for 6 h in air atmosphere. The obtained zeolite was ion-exchanged with NH_4Cl twice, and the final product was denoted as HZSM-5.

Synthesis of supported 5 wt% Ru/HZSM-5

The supported 5 wt. % Ru catalysts were prepared by incipient wetness impregnation. Firstly a solution of $RuCl_3 \cdot 3H_2O$ (6.35 mL, conc: 0.040 g/L) was added drop-wise to an aqueous suspension (150 mL H_2O, 2.0 g support) with stirring at room temperature overnight. Afterwards,

the as-formed catalysts were filtered, dried at 80 °C overnight. Finally, it was calcined in flowing N_2 (flowing rate: 100 mL/min) at 350 °C for 4 h, and reduced in flowing hydrogen (flowing rate: 100 mL·min^{-1}) at 350 °C for 4 h.

Catalyst characterization

The amounts of Si, Al, and Ru were quantified by inductively coupled plasma (ICP) atomic emission spectroscopy on a Thermo IRIS Intrepid II XSP. The crystal morphology and size were determined by scanning electron microscopy (SEM) on a Hitachi S-4800 microscope and transmission electron microscopy (TEM) on a JEOL JEM-2100 microscope at an accelerating voltage of 200 kV.

Nitrogen sorption isotherms were obtained at 77 K using a BELSORP-MAX instrument after degassing the samples for 10 h under vacuum at 573 K. The surface areas were calculated by the Brunauer-Emmett-Teller (BET) method. X-ray diffraction (XRD) patterns were obtained with a Rigaku Ultima IV X-ray diffractometer (35 kV and 25 mA) using Cu Kα radiation (λ = 1.5405 Å) over a 2θ ranging from 10° to 70° at a scanning speed of 60° min^{-1}. The TPR-H_2 profile was recorded at a heating rate of 5 K min^{-1} from 293 to 1073 K by using Micromeritics tp5080 apparatus equipped with a thermal conductor detector (TCD).

The IR spectra of the adsorbed CO (IR-CO) were recorded with a Nicolet NEXUS 670 FTIR spectrometer equipped with an in situ IR cell. The samples were reduced in H_2 at 623 K for 1 h and then adsorbed CO at room temperature. The IR spectra of the adsorbed pyridine (IR-Py) were measured on a Nicolet Fourier transform infrared spectrometer (NEXUS 670) equipped with an in situ IR cell. The samples were activated in a vacuum at 823 K for 1 h before equilibration with pyridine at 423 K, and then evacuated at 423 K for 1 h.

X-ray photoelectron spectroscopy (XPS) were worked with Al Kα (hv = 1486.6 eV) radiation with a Thermo Scientific K-Alpha spectrometer. Charging effects were corrected by using the C 1s peak due to adventitious carbon with EB fixed at 284.8 eV.

The IR spectra of the adsorbed guaiacol were obtained by Bruker Tensor 27 equipped with an in situ IR cell. The samples were activated in He at 773 K for 1 h. After cooling to room temperature, the samples were exposure guaiacol adsorption at room temperature until adsorption saturation. Then the samples were treated by flowing He at room temperature to remove the physically adsorbed guaiacol.

The TPD/H_2-MS experiments were done with the AMETEK DYCOR quadrupole mass spectrometer (QMS). The samples were activated at 673 K for 1 h by vacuum pump and then reduced in H_2 at 673 K for 1 h. After cooling to ambient temperature, the samples were exposed to H_2 till adsorption saturation. Subsequently the samples were flowed by N_2 with a flowing rate: 20 mL·min^{-1} at room temperature to remove the physically adsorbed H_2. Then the H_2 signal was detected by QMS with a heating rate of 5 K·min^{-1}.

Catalytic testing

Reactions on guaiacol or other phenolic monomers: In a typical reaction, guaiacol (1.0 g), Ru/HZSM-5 (0.05 g), and deionized water (100 mL) were charged into a batch autoclave (Parr Instrument, 300 mL). After the reactor was flushed with N_2 at room temperature for three times, the autoclave was charged with 6 bar N_2 and 2 bar H_2, and the reaction was conducted at 240 °C with a stirring speed of 600 rpm. After reacting, the liquid products were extracted using ethyl acetate and analyzed by GC and GC-MS. For analysis, an internal standard dodecane was added to calculate the carbon balance. Conversion = (weight of converted reactant/weight of the starting reactant) × 100%. Yield of liquid products (C%) = (C atoms in liquid products/C atoms in the starting reactant) × 100%. Selectivity (C%) = (C atoms of each product/C atoms in all the liquid products) × 100%.

The recycling tests for guaiacol conversion with Ru/HZSM-5: the Ru/HZSM-5 catalyst was examined in four consecutive catalytic runs for guaiacol HDO by employing a batch of Ru/HZSM-5 catalyst at 240 °C and 2 bar H_2 for 1 h. After each reaction, the used Ru/HZSM-5 catalysts were filtered and then dried at 60 °C in vacuum before next catalytic runs.

Acknowledgements

This research was supported by the Key Research and Development Program of the Ministry of Science and Technology (Grant No. 2016YFB0701100), the Recruitment Program of Global Young Experts in China, National Natural Science Foundation of China (Grant No. 21573075), the Shanghai Pujiang Program (Grant No. PJ1403500), and the Foundation of Key Laboratory of Low-Carbon Conversion Science & Engineering, Shanghai Advanced Research Institute, Chinese Academy of Sciences.

Keywords: Selective hydrogenolysis • arenes • lignin • HZSM-5 morphology • Aqueous phase reaction

[1] F. D. M. Mercader, M. J. Groeneveld, S. R. A. Kersten, C. Geantet, G. Toussaint, N. W. J. Way, C. J. Schaverien, K. J. A. Hogendoorn, *Energy Environ. Sci.* **2011**, *4*, 985-997.

[2] a) Y. Wang, S. De, N. Yan, *Chem. Commun.* **2016**, 52, 6210-6224. b)D. D. Laskar, M. P. Tucker, X. Chen, G. L. Helms, B. Yang, *Green Chem.* **2014**, *16*, 897-910; c) H. Northwest, J. Male, Y, Wang, *ACS Catal.* **2013**, *3*, 1047-1070; d) G. Yao, G. W, W. Dai, N. Guan, L. Li, *Fuel* **2015**, *150*, 175-183; e) J. Kong, M. He, J. A. Lercher, C. Zhao, *Chem. Commun.* **2015**, *51*, 17580-17583; f) J. Zhang, C. Zhao, *Chem. Commun.* **2015**, *51*, 17249-17252; g) B. Ma, J. Hu, Y. Wang, C. Zhao, *Green Chem.* **2015**, *17*, 4610-4617; h) J. Zhang, C. Zhao, *ACS Catal.* **2016**, *6*, 4512-4525; i) B. Ma, X. Yi, L. Chen, A. Zheng, C. Zhao, *J. Mater. Chem. A* **2016**, *4*, 11330-11341; j) B. Ma, C. Zhao, *Green Chem.* **2015**, *17*, 1692-1701; k) J. Kong, B. Li, C. Zhao, *RSC Adv.* **2016**, *6*, 71940-91951; l) B. Ma, H. Cui, C. Zhao, *Chem. Commun.*, **2017**, 53, 10358-10361; m) B. Ma, H. Cui, D. Wang, P. Wu, C. Zhao, *Nanoscale* **2017**, *9*, 5986-5995; n) B. Li, L. Li, C. Zhao, *Green Chemistry*, **2017**, doi: 10.1039/C7GC02414B; o) L. Wu, L. Li, B. Li, C. Zhao, *Chem. Commun.*, **2017**, 53, 6152-6155; p) Z. Luo, Z. Zheng, L. Li, Y. Cui, C. Zhao, *ACS Catal.* **2017**, 7, 8304-8313.

[3] a) A. Corma, S. Iborra, A. Velty, *Chem. Rev*. **2007**, *107*, 2411-2502; b) M. Stocker, *Angew. Chem. Int. Ed*. **2008**, *47*, 9200-9211J; c) Zakzeski, P. C. A. Bruijnincx, A. L. Jongerius, B. M. Weckhuysen, *Chem. Rev.* **2010**, *110*, 3552-3599; d) T. P. Vispute, H. Zhang, A. Sanna, R. Xiao, G. W. Huber, *Science* **2010**, *330*, 1222-1227; e) M. Saidi, F. Samimi, D. Karimipourfard, T. Nimanwudipong, B. C. Gates, M. R. Rahimpour, *Energy Environ*. *Sci.* **2014**, *7*, 103-129.

[4] M. Ferrari, R. Maggi, B. Delmon, P. Grange, *J. Catal.* **2001**, *198*, 47-55.

[5] A. Centeno, E. Laurent, B. Delmon, *J. Catal.* **1995**, *154*, 288-298.

[6] a) T. Nimmanwudipong, C. Aydin, J. Lu, R. C. Runnebaun, K. C. Brodwater, N. D. Browning, D. E. Block, B. C. Gates, *Catal. Lett.* **2012**, *142*, 1190-1196; b) M. A. Gonzalez-Borja, D. E. Resasco, *Energy Fuels* **2011**, *25*, 4155-4162.

[7] M. V. Bykova, D. Y. Ermakov, V. V. Kaichev, O. A. Saraev, M. Y. Lebedev, V. A. Yakovlev, *Appl. Catal. B,* **2012**, *113*, 296-307.

[8] R. N. Olcese, M. Bettahar, D. Petitjean, B. Malaman, F. Giovanella, A. Dufour, *Appl. Catal. B* **2012**, *115*, 63-73.

[9] J. Chang, T. Danuthai, S. Dewiyanti, C. Wang, A. Borgna, *ChemCatChem* **2013**, *5*, 3041- 3049.

[10] J. Sun, A. M. Karim, H. Zhang, L. Kovarik, X. S. Li, A. J. Hensley, J. S. Mcewen, Y. Wang, *J. Catal.* **2013**, *306*, 47-57.

[11] C. Sepulveda, K. Leiva, R. Garcia, L. R. Radovic, I.T. Ghampson, W. J. Desisto, J. L. G. Fietto, N. Escalona, *Catal. Today* **2011**, *172*, 232-239.

[12] M. Selvaraj, K. Shanthi, R. Maheswari, A. Ramanathan, *Energy Fuels* **2011**, *25*, 4155-4162.

[13] J. S. Moon, E. G. Kim, Y. K. Lee, *J. Catal.* **2014**, *311*, 144-152.

[14] a) Z. Luo, C. Zhao, *Catal. Sci. Technol.* **2016**, *6*, 3476–3484; b) Z. Luo, Y. Wang, M. He, C. Zhao, *Green Chem.* **2016**, *18*, 433–441.

[15] Z. Luo, Z. Zheng, Y. Wang, G. Sun, H. Jiang, C. Zhao, *Green Chem.* **2016**, *18*, 5845-5858.

[16] Y. Huang, L. Yan, M. Chen, Q. Guo, Y. Fu, *Green Chem.* **2015**, *17*, 3010.

[17] K. Hadjiivanov, J. C. Lavalley, J. Lamotte, F. Maugé, J. Saint-Just M. Che, *J. Catal.* **1998**, *176*, 415−425.

[18] C. Chiu, A. Genest, A. Borgna, N. Rösch, *ACS Catal.* **2014**, *4*, 4178-4188.

[19] J. Lu, A. Heyden, *J. Catal.* **2015**, *321*, 39-50.

[20] A. Popov, E. Kondratieva, J. M. Goupil, L. Mariey, P.Bazin, J. Gilson, A. Travert, F. Mauge, *J. Phys. Chem. C* **2010**, *114*, 15661–15670.

[21] a) G. Neri, A. M. Viso, A. Donato, C. Milone, M. Malentacchi, G. Gubitosa, *Appl. Catal. A*, **1994**, *110*, 49-59；b) W. Song, Y. Liu, E. Barath, C. Zhao, J. A. Lercher, *Green Chem.* **2015**, *17*, 1204-1218.

[22] D. Wang, B. Ma, B. Wang, C. Zhao, P. Wu, *Chem. Commun.* **2015**, *51*, 15102-15105.

[23] J. Ding, M. Wang, L. M. Peng, N. H. Xue, Y. M. Wang, M. Y. He, *Appl. Catal. A: Gen* **2015,** *503,* 147-155.

10.1002/cctc.201701398

WILEY-VCH

Entry for the Table of Contents

FULL PAPER

Morphologically cross-shaped HZSM-5 loaded Ru nanoparticles have demonstrated high activity (rate: 7.8 $g \cdot g^{-1} \cdot h^{-1}$) in selective hydrogenolysis of guaiacol to benzene in water with a nearly quantitative yield accompanied with high durability.

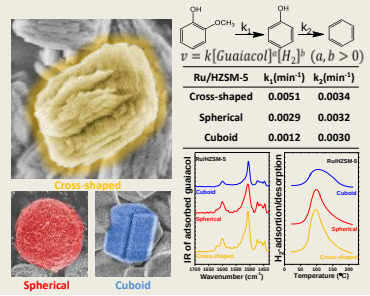

*Zhaoxia Zheng, Zhicheng Luo, Chen Zhao**

Page No. – Page No.

Morphologically Cross-shaped Ru/HZSM-5 Catalyzed Tandem Hydrogenolysis of Guaiacol to Benzene in Water